International Journal of Fatigue 173 (2023) 107701

Contents lists available at ScienceDirect

International Journal of Fatigue

journal homepage: www.elsevier.com/locate/ijfatigue

Uniaxial plastic strain effect on the corrosion-fatigue resistance of ISO 5832-1 stainless steel biomaterial

William Naville [a,b,*], Rodrigo Magnabosco [a], Isolda Costa [b]

[a] Centro Universitário FEI, Departamento de Engenharia de Materiais, São Bernardo do Campo, SP, Brazil
[b] Instituto de Pesquisas Energéticas e Nucleares, São Paulo, SP, Brazil

ARTICLE INFO

Keywords:
Corrosion fatigue
Environmental assisted fatigue
Stainless steel
Hydrogen peroxide
Albumin pH 3.0

ABSTRACT

Orthopaedic implants are used for fracture stabilization or orthopaedic reconstruction. During implantation and even in the implant accommodation process, there may be plastic strain and induction of residual stresses. This information creates a test procedure involving pre-strain, pre-conditioning in the corrosive environment and corrosion-fatigue tests. Two solutions were used, PBS (phosphate-buffered saline, neutral pH, recommended for corrosion evaluation tests) and SHA (saline solution with hydrogen peroxide and albumin pH 3.0). The results showed that, differently from PBS, SHA promoted localized corrosion, reducing fatigue resistance in all tested conditions. In addition, plastic pre-strain influenced the failure process.

1. Introduction

Internal fixation devices are orthopaedic implants designed to provide temporary stabilization. They are used to maintain the shape of the reconstructed bone in fracture treatment or orthopaedic reconstruction surgical procedures. Implants are commonly constructed using biocompatible austenitic stainless steel and are removed after reaching their purpose [1].

Austenitic stainless steels (ASS) present excellent mechanical properties for application as biomaterials. Due to their paramagnetic behaviour, these steels are also safe in magnetic resonance imaging procedures [2], making their use highly attractive. However, they are not immune to corrosion, and the most common is the occurrence of localized corrosion; in ASS, pitting corrosion is the usual occurrence. It is also one of the most severe forms of localized corrosion and adversely affects biocompatibility and mechanical strength. Biocompatibility is a crucial characteristic that biomaterials must present in orthopaedic applications, not adversely affecting the local system of the host medium [3].

The main problem in the study of pitting corrosion is its stochastic initiation nature. Despite many research works, the pitting initiation mechanism is not fully understood, and several initiation mechanisms have been proposed [4,5]. Pitting mechanisms depend on the environment to which the metallic material is exposed. In the case of biomaterials, the environment is the highly complex body fluids.

The human body fluids contain an extensive range of biological molecules such as proteins, mainly albumin, and cellular physiology products as reactive oxygen species, including hydrogen peroxide (H_2O_2), making these environments corrosive to metallic alloys. Internal implants are exposed to this kind of environment. A pH decrease occurs in the implants' areas, mainly in the initial periods after implantation, usually associated with inflammatory processes. Commonly, the pH of body fluids is neutral (7.2–7.4), but in the implanted areas, it may drop to nearly 2.5 [1,6–11]. The local pH decrease makes the environment even more aggressive to implants and might lead to localized corrosion.

Eventually, straight bony plates that act as internal fixation devices are deformed to shape the curvature of the bone during surgical procedures. This deformation requires material ductility [12]. However, strain hardening caused by plastic deformation changes the metallurgical properties of stainless steels, altering their hardness, yield limit, surface roughness and, ultimately, corrosion resistance.

Besides corrosion, internal fixation devices are also subjected to mechanical cyclic loading that causes the movement and creation of crystalline defects, even below the yield limit. Yield occurs preferentially in certain crystal slip planes, creating persistent slip bands (PSBs), which evolve from extrusions and intrusions and generate persistent macro bands (PMBs). These can occur preferentially at the surface, grain boundaries, an interface between inclusions and matrix and at defects, such as pits, resulting in a high-stress level and consequently amplifying this phenomenon. Fatigue cracks nucleate from PMBs and propagate

* Corresponding author.
E-mail addresses: wnaville@fei.edu.br, wnaville@gmail.com (W. Naville).

https://doi.org/10.1016/j.ijfatigue.2023.107701
Received 22 December 2022; Received in revised form 17 March 2023; Accepted 22 April 2023
Available online 26 April 2023

until failure [13,14].

Mechanical cyclic loading associated with corrosion phenomena helps the mechanisms that lead to failure. Thus, implant failures can result from the interaction of fatigue and corrosion processes. During cyclic fatigue loading, the localized and subsequent passive film breakdown can accelerate crack initiation and localized corrosion (pitting). Those occurrences can enhance local stress concentration and the beginning and propagation of fatigue cracks [15,16]. In corrosive environments, corrosion can increase surface roughness, create local stress concentration, and facilitate fatigue crack initiation. The transport of species from the corrosion medium to the surface close to the slip bands also enhances crack start [13,17–19].

A 10-year retrospective of knee and hip replacement surgeries found that femoral fractures increased after these types of surgery. The treatment of these fractures commonly uses bone plates. The plates presented defects in seven out of eighty patients, and replacement surgeries were necessary. The mean hospital stays time of those surgeries, in the case of the femur fracture, was (20 ± 9) days after the replacement of the knee joint and (22 ± 14) days after the replacement of the hip joint [20].

The literature on the corrosion-fatigue data of the ISO 5832-1 ASS considers the implantation and postoperative conditions, like plastic pre-strain and the roughness generated from this pre-strain. Recovery time is not found in extensive research. For the design of biocompatible internal fixation devices, corrosion-fatigue tests that consider conditions as close as possible to real applications are necessary. This work aims to produce corrosion-fatigue data for the ISO 5832-1 austenitic stainless steel under conditions similar to those found during application. This study also investigates the effect of plastic pre-strains imposed by compression or tension strains; it uses pre-conditioning test conditions that simulate the recovery period before the patient's movement.

2. Material and methods

2.1. Material

The material used in this work was the ISO 5832-1 austenitic stainless steel (ASS) provided as 15.87 mm diameter bars in the solution-treatment condition by Villares Metals, Brazil. The chemical analysis of the steel was carried out according to ASTM E1097 [21] and E1019 [22] standards using Continuous Current Plasma Atomic Emission Spectrometry (ICPE-9000 equipment, Shimadzu) and Fusion and Combustion techniques (LECO CS230 equipment).

2.2. Microstructural analysis

Microstructural analysis of the ASS was performed according to ASTM E3 [23]. Nonmetallic inclusion content was estimated by ASTM E45 - Method D [24] using an Olympus Optical Microscope with image acquisition and analysis software. Electrolytic etching in 10% oxalic acid solution under 15 Vcc for 60 s was conducted for microstructure observation. Grain size in the longitudinal and transverse directions was measured according to the ASTM E112 - Mean Intercept Method [25].

2.3. Tension and fatigue test specimens

Standard-sized tension test specimens were machined with the dimensions shown in Fig. 1a, following ASTM E8M standard [26]. A uniaxial fatigue test with load control was carried out according to ASTM E466 [27] standard, with fully reversed loads. Test specimens of lenticular circular cylindrical hourglass type, with dimensions shown in Fig. 1b were used. The area for exposure to the test solution was ground to 1200 mesh sandpaper and then polished with diamond suspension until 1 μm finishing, using water as a lubricant. No scratches perpendicular to the longitudinal axis were found after polishing.

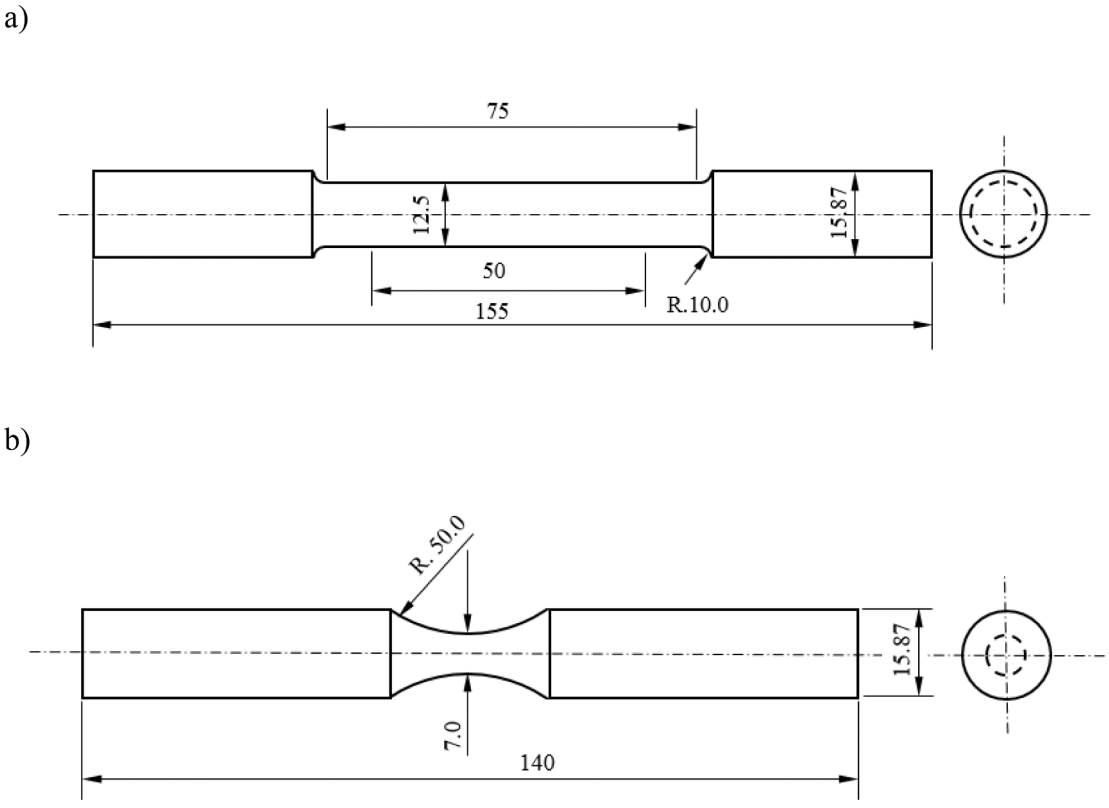

Fig. 1. a) tension test specimen and b) uniaxial fatigue test specimen. Dimensions are expressed in millimeters.

2.4. Pre-strain

ASS pre-strain samples were obtained to simulate the strain effects imposed during surgery procedures by physicians to set the implant during operation. There is no usual strain. It depends on the geometry of the implant and the fracture stabilization conditions during surgery, which can be a large range of strain. However, in the test, the specimen's geometry does not allow a large strain range and the maximum strain was chosen without compromising its alignment. Exploratory investigations were performed to prevent geometric instability (buckling) during compression (imposed during plastic pre-strain of specimens or fatigue tests). A maximum compression strain of 15% was found to prevent buckling.

Solution-treated and polished (SPC) specimens were used in corrosion-fatigue tests without plastic strain. The other corrosion-fatigue specimens were exposed to plastic pre-strain under tension stress (PPUT) or compression stress (PPUC). PPUT and PPUC were pre-strained until a 15% strain (in tension or compression) was achieved.

Pre-strain was performed in uniaxial tension or compression tests in an MTS 810-250kN equipment, also used for monotonic and fatigue tests. Monotonic loads were applied according to ASTM E8M and E9 standards [26,28], and fatigue tests followed ASTM E466 [27].

2.5. Test solutions and pre-conditioning

A test solution composed of a solution named PBS, phosphate-buffered saline neutral pH, and a solution called SHA, saline solution with peroxide and albumin (0.9% NaCl, 1% H_2O_2 and 1% albumin, pH 3 adjusted with H_2SO_4), were chosen to simulate physiological fluids found around implants during the post-operation period. The ASS fatigue specimens (SPC, PPUT and PPUC) were exposed to the test solution for 21 days before the corrosion-fatigue test to simulate the post-operative period after implant, simulating the patient stays on rest after surgery. In this period, the implant is in contact with body fluids, but it does not suffer the action of cyclic loading. During this period, the test solution was recirculated through the ASS specimens using a pump that allowed the solution to contact the useful region of the specimen. The aim was to avoid the attack on the unpolished areas. The flow of the solution was set in laminar mode, and a temperature controller coupled to a Pt-100 thermocouple controlled the solution temperature at (37 ± 1) °C.

2.6. Residual stress and crystal structure

The specimens' longitudinal direction residual stress analysis was performed using the X-ray diffractometer Shimadzu XRD-7000 (Cr Tube). The same surface region indicated in Fig. 2a was positioned to coincide with the point of incidence of the X-ray beam. The same experimental arrangement was used to identify phases by X-ray diffraction, and these measurements have been confirmed with the Helmut Fischer MP30 ferritscope. Due to the geometry of the specimens, precisely their length, measuring the residual stress in the circumferential direction was impossible.

2.7. Hardness test

As described in ASTM E384 standard [29], Vickers microhardness measurements were carried out along the entire useful region of specimens, in both conditions, solution-treated and plastic pre-strained. Measurements were taken at longitudinal sections of the fatigue specimens, at 7 points along with the plastic pre-strained extent of the useful area, with a spacing of approximately 0.5 mm each, as illustrated in Fig. 2. The microhardness measurements were performed with a Shimadzu HMV-2 micro-durometer, using 4.905 N load.

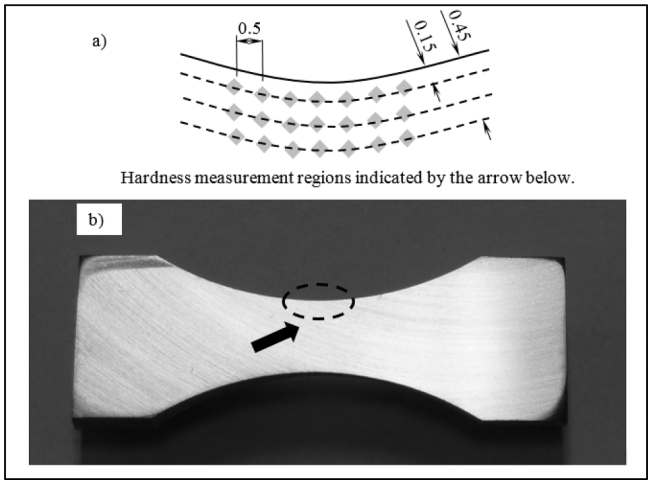

Fig. 2. a) schematic representation of the area of microhardness measurements; b) area used for microhardness measurements shown in one of the sectioned test specimens.

2.8. Corrosion-fatigue test

The corrosion-fatigue test was performed according to ASTM E466 [27], and the experimental setup is shown in Fig. 3. A tube was mounted around the useful area of the specimen and sealed by flexible rings. This tube was connected to a tank with a temperature control system (37 ± 1) °C. A pump for solution recirculation was used to obtain a laminar flow on the specimen at a temperature of 36.5 ± 1 °C. Concurrently, completely reversed cyclic loads were applied at 3 Hz. The strain was monitored to detect the start of failure. Since the cross-section of the hourglass specimen is small, the appearance of a visually detectable crack was used as a failure criterion.

2.9. Surface aspects

The failures and surface conditions were characterized using: a Zeiss Stemi 2000-C stereomicroscope, an Olympus optical metallographic microscope, a Shimadzu CamScan 3200 LV Scanning Electron Microscope, and a Shimadzu Atomic Force Microscope SPM-9600. These evaluations were performed to understand the failure initiation by corrosion-fatigue. Surfaces were observed before and after the failure of the specimens.

Roughness surface measurements were performed using an Atomic Force Microscope (AFM). The specimens' plastically deformed cross sections were carefully cut to remove a small, intact and representative area of that surface, where the measurements were made before any fatigue test.

3. Results

3.1. Chemical and microstructure results

Chemical analysis results in Table 1 showed that the alloy was according to ISO 5832-1 standard [30]. Fig. 4a presents the longitudinal section of a polished specimen, showing fine inclusions of D type - Globular Series 1, predominantly oxides, according to ASTM E45 standard [24]. Fig. 4b-4d show the equiaxed grains microstructure of the SPC, PPUC and PPUT samples. Metallographic etching revealed grain boundaries, and in the pre-strain-free solution-treated condition, the grain size in the longitudinal direction measured 12.8 ± 0.3 μm. However, the grains of the specimens exposed to plastic compression strain (PPUC) were slightly flattened in the longitudinal direction (grain size of 10.2 ± 0.5 μm), parallel to the horizontal in the micrographs (Fig. 5c). In contrast, the grains of tension plastic pre-strained samples (PPUT) were

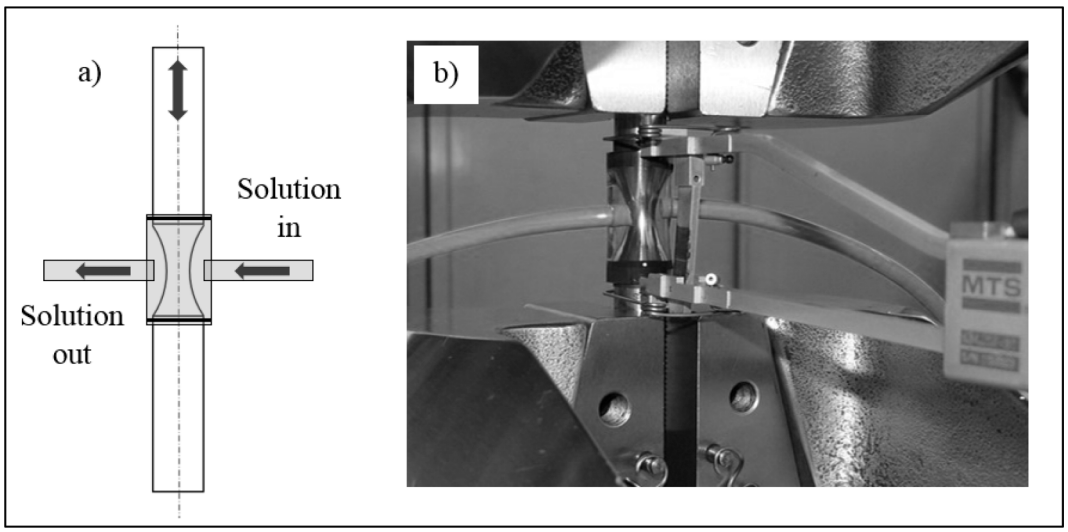

Fig. 3. a) schematic assembly and b) actual test equipment assembly.

Table 1
Chemical composition (wt. %) of the ISO 5832-1 used and that of the standard. Balance was Fe.

	Elements (wt. %)								
	C	**Si**	**Mn**	**Cr**	**Ni**	**P**	**S**	**Mo**	**Cu**
Material	0.019	0.28	1.69	17.0	13.7	0.034	<0.001	2.87	0.07
ISO 5832-1 Standard	<0.03	<1.0	<2.0	17.0-19.0	13.0-15.0	<0.025	<0.01	2.25-3.00	<0.5

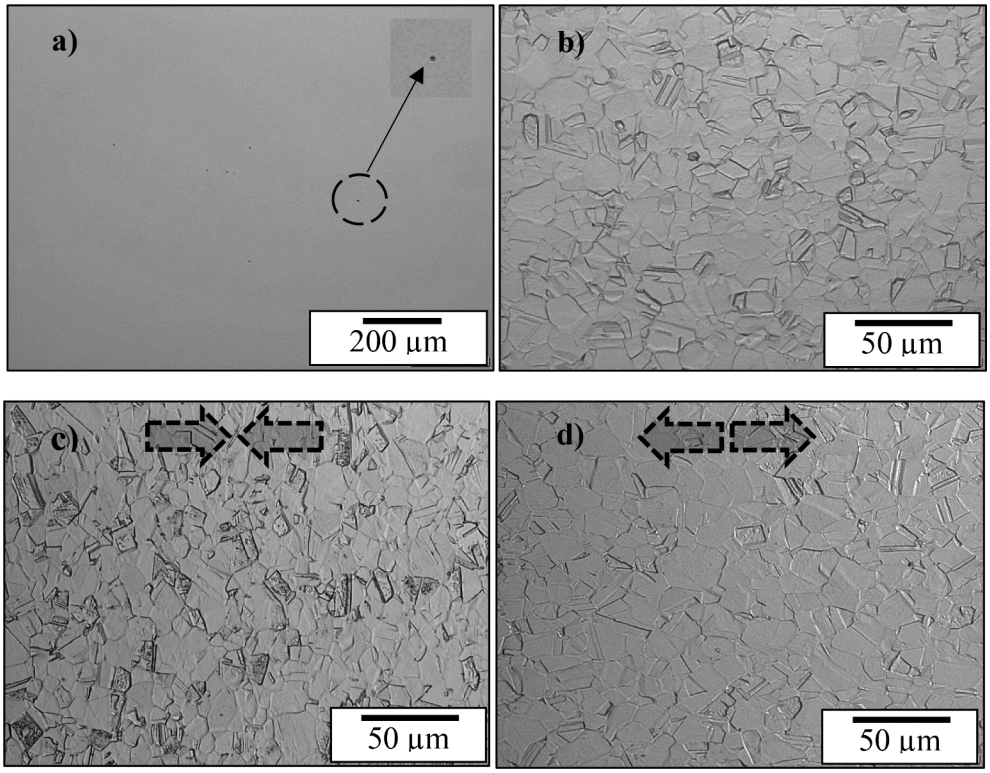

Fig. 4. ISO 5832-1 microstructure, specimens in the longitudinal direction, (a) without etching (showing inclusions), and after etching of (b) solution-treated (SPC), (c) pre-strained under compression stress (PPUC) and d) pre-strained under tension stress (PPUT).

slightly elongated (grain size of 14.2 ± 1.6 µm) (Fig. 5d). In the transverse direction, the results showed that no variation was obtained in the annealed condition 11.4 ± 1.1 µm, compressed state 11.6 ± 0.9 µm and tensioned 11.8 ± 0.8 µm. Scanning the entire longitudinal section of the specimens indicated a homogeneous microstructure, with the plastic pre-strain restricted to the area exposed to corrosion-fatigue tests, which

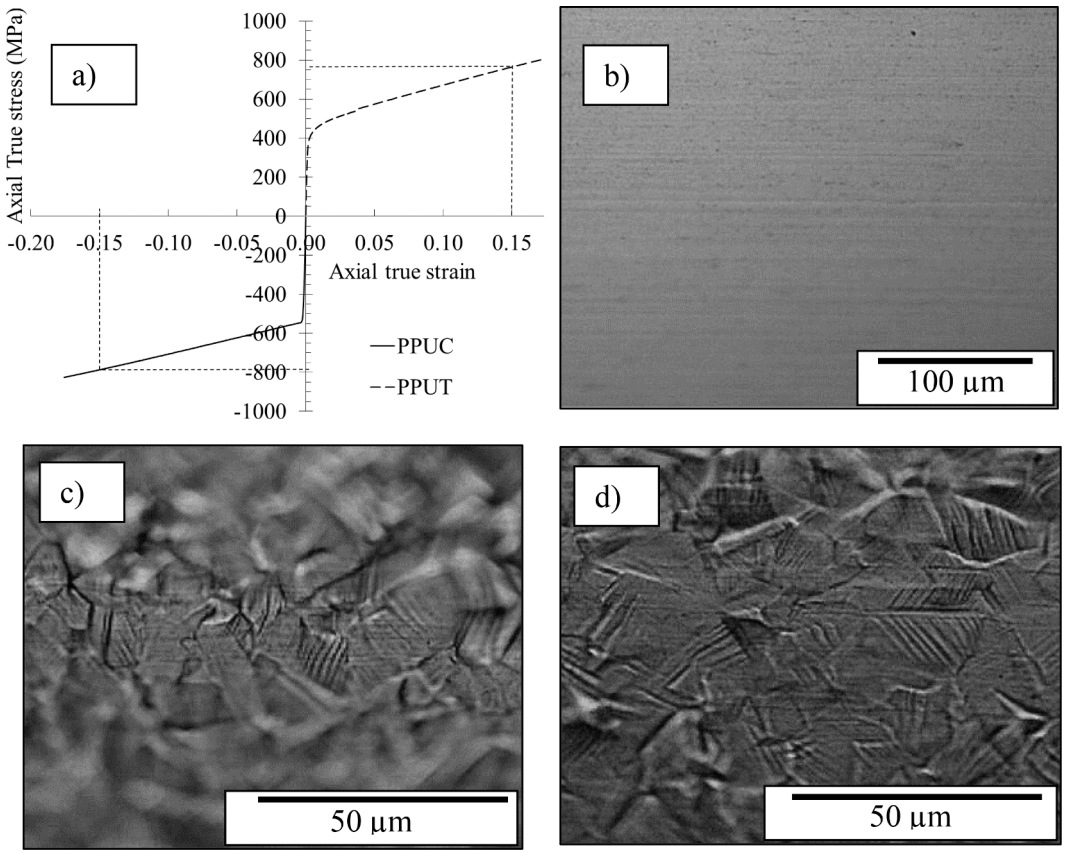

Fig. 5. a) stress–strain curve relative to the deformation process before corrosion-fatigue tests, b) polished surface specimen, c) polished surface and pre-strained under tension specimen (PPUT) and d) polished surface and pre-strained under compression specimen (PPUC).

allows the evaluation of the applied plastic pre-strain on the corrosion-fatigue of the ASS.

3.2. Plastic Pre-strain cold work and residual stress

The mean hardness values obtained for the plastic pre-strained samples under compression are (264 ± 6) HV0.5 and under tension (270 ± 6) HV0.5. This result showed similar hardness for both conditions. The hardness of the samples exposed to plastic pre-strain was increased by approximately 40% relative to the solution-treated ones (193 ± 5 HV0.5). Tension test results of the solution-treated condition are shown in Table 2. The properties specified by ISO 5832-1 standard show that the mechanical properties of the solution-treated ASS [30] are in the specification for the annealed condition.

Fig. 5a shows two examples of the true stress–strain curves obtained during the deformation process before corrosion-fatigue tests. The plastic pre-strain of approximately 15% in tension in the upper right quadrant indicates true stress of roughly 770 MPa. In the lower-left quadrant, the plastic pre-strain of 15% in compression resulted in true stress of approximately 786 MPa.

Fig. 5b shows the polished surface specimen before the uniaxial plastic pre-strain process. Mechanical polishing resulted in a surface free from scratches in the cross direction of load application. The tension or compression plastic pre-strain, Fig. 5 c and 5d, respectively, shows that slip planes produced steps on the polished surface, affecting microstructural constituents (grains and slip bands) and altering surface roughness. This effect was better visualized in the optical microscope; as the cylindrical surface, an out-of-focus region was produced. Table 3 shows the mean roughness values for the three types of surfaces used in this study, determined by Atomic Force Microscopy (AFM), confirming the change in roughness caused by the plastic pre-stain of ASS.

The residual stress values determined in the longitudinal direction of the specimens using X-ray diffraction for the samples in the solution-treated conditions and plastically pre-strained in tension and compression are also shown in Table 3. Note that the residual stress determined was more compressive with a uniaxial plastic pre-strain of 15% in compression. In comparison, with the application of the uniaxial plastic

Table 3
Mean roughness (Ra) values of the various types of specimens tested.

Specimen	Roughness (Ra max.) mean values	Longitudinal Residual Stress
SPC	(10 ± 5) nm	−166 ± 8 MPa
PPUC	(250 ± 28) nm	−347 ± 87 MPa
PPUT	(110 ± 10) nm	284 ± 41 MPa

Table 2
Mechanical properties of the ISO 5832-1 ASS in the solution-treated condition.

	S_y(MPa)	S_r(MPa)	E(%)	AR(%)	H(MPa)	n	σ_f(MPa)	ε_f
Specimen ISO 5832-1	407 ± 3	654 ± 7	47 ± 2	77 ± 2	1117 ± 22	0.2245 ± 0.0079	1272 ± 56	1.48 ± 0.10
Standard (Annealed)	>190	490-690	>40	–	–	–	–	–

pre-strain of 15 % in traction, the residual stress was more tractive.

3.3. Pre-conditioning effect and corrosion fatigue results

Pre-conditioning effect

After the pre-conditioning period, the areas equivalent to those shown in Fig. 5 were inspected. Neither localized nor uniform corrosion was found in both solutions and conditions. After 21 days of contact with the solutions, the surface of the specimens did not show signs of corrosive attack. Both the previously deformed regions and the previously polished regions presented the same aspect.

Corrosion fatigue results

The effect of hardening on corrosion-fatigue resistance in PBS solution is presented in Fig. 6a. It shows a significant increase in resistance concerning the solution-treated condition. Similar effects of increased corrosion-fatigue resistance by hardening were observed in SHA solution, Fig. 6b. Adopting a life estimate of 300,000 cycles for comparison, under PBS solution, mechanically polished and plastic pre-strained in compression (PPUC) specimens showed 25% higher corrosion-fatigue resistance, while polished and plastic pre-strained in tensile (PPUT) showed an increase 30%, both compared to solution-treated condition. This same analysis showed a 35% increase in corrosion-fatigue strength in the SHA solution for both conditions.

It was notable that, contrary to the previous conditioning stage, during which this ASS supported contact with the solutions without surface attack damage, this behavior changes when the cyclic test starts, and corrosion starts to have a remarkable role. In this cyclic loading condition, the different solutions presented different mechanisms of superficial attacks that triggered the decrease in fatigue resistance. The attack was uniform in the PBS solution, and localized corrosion was observed in the SHA solution.

A comparison of the effect of the test solution on the fatigue behavior for the three types of specimen conditions tested is shown in Fig. 7. Fatigue resistance is reduced in SHA solution comparatively to PBS solution in all conditions, Fig. 7a, b and c. A decrease in fatigue resistance exponent b in the SHA solution shows the corrosiveness effect of this test solution. It is noted that with stress decrease, there is a tendency for the number of cycles until failure decreases, compared with the PBS solution. Results can be explained by the greater corrosivity of the SHA solution; consequently, the effect of corrosion on the appearance and progression of the failure in the corrosion-fatigue process. For 300,000 cycles on SPC condition, the decrease in corrosion-fatigue life was 11%. The corrosion-fatigue resistance drop in the PPUT condition was 8.6%, slightly lower than the SPC condition, indicating less influence of

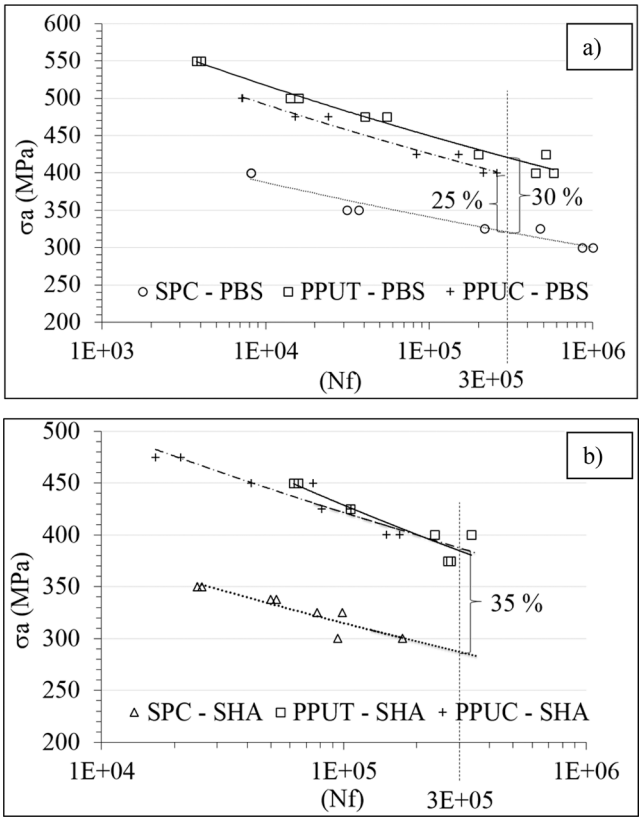

Fig. 6. Solution-treated corrosion-fatigue test (SPC), pre-strained under tension stress (PPUT) and pre-strained under compression stress (PPUC) specimens tested in a) PBS solution and b) SHA solution.

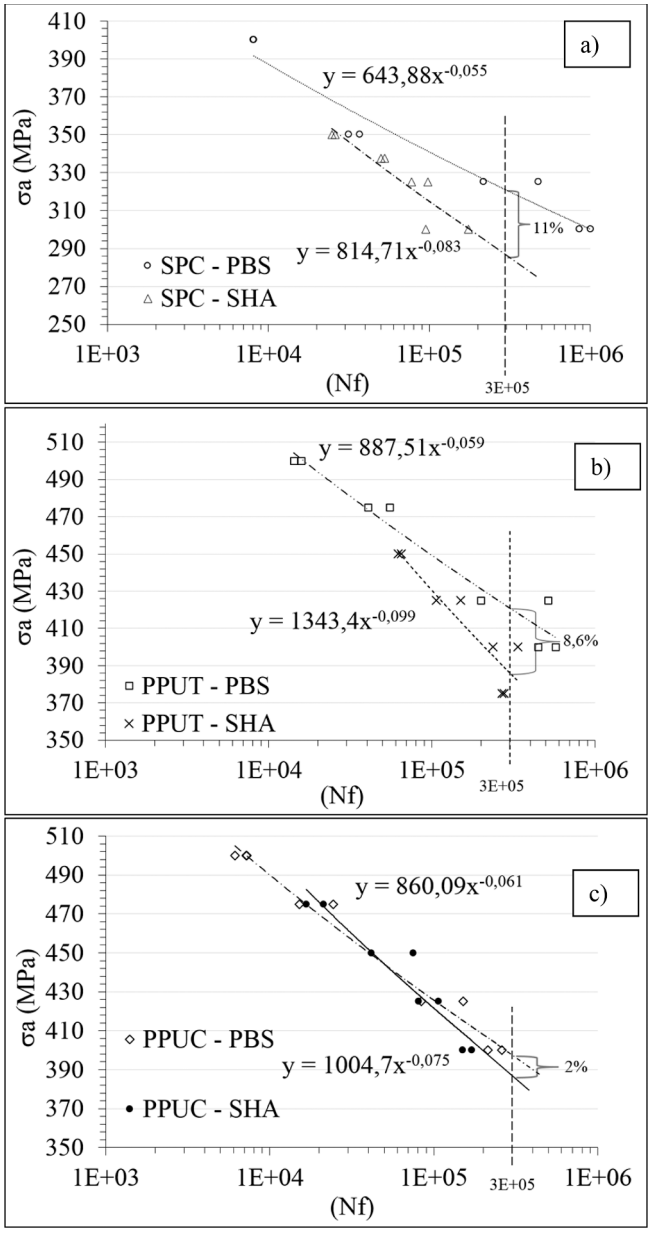

Fig. 7. Corrosion-fatigue test. a) Solution-treated in PBS (SPC-PBS) and solution-treated in SHA (SPC-SHA). b) Pre-strained under tension stress in PBS (PPUT-PBS) and pre-strained under tension stress in SHA (PPUT-SHA). c) Pre-strained under compressive stress in PBS (PPUC-PBS) and pre-strained under compressive stress in SHA (PPUT-SHA).

corrosion in the PPUT condition. However, that would be a relevant difference. By calculating the fatigue life estimate dispersion for 300,000 cycles, according to the ASTM E739 standard [31], ± 2.8% is obtained for the PPUT - PBS condition and ± 3.3% for the PPUT - SHA condition. Thus, in the worst case, we would have a dispersion of 6.1%, less than the difference of 8.6%, which corroborates the statement of a small influence on the corrosion-fatigue resistance in this condition. In the case of mechanically polished and pre-deformed compression (PPUC) condition, for 300,000 cycles, the drop in corrosion-fatigue resistance was 2%, lower and not statistically relevant compared to the other two conditions, SPC and PPUT, indicating less influence of corrosion in the PPUC condition.

Crack initiation in PBS solution

Fractographic analysis was performed on specimens that remained longer during the corrosion-fatigue test in contact with PBS solution. The fracture surface of the pre-strained specimen under tension stress, which resisted 199,912 cycles (18.5 h under 425 MPa stress amplitude), can be observed in Fig. 8a. Fatigue fracture with nucleation and propagation from the surface, as observed, was common in fatigue failure mechanisms. There was no evidence of localized corrosion in specimens subjected to this solution, such as pitting or intergranular attack. Similarly, analysis of the fractured surfaces of specimens pre-strained under compression stress after 151,037 cycles (14 h under 425 MPa stress amplitude) and solution-treated ones after 474,736 cycles (44 h under 325 MPa stress amplitude) showed that all followed the same failure mechanism, which is fatigue fracture with nucleation and propagation from the surface. Thus, uniform surface corrosion in synergy with cyclic surface strain was probably the cause of the reduction in fatigue strength.

Crack initiation in SHA solution

Fractographic analysis in Fig. 8b shows a specimen submitted to corrosion-fatigue test in SHA solution that failed after 81,088 cycles (7.5 h under 425 MPa stress amplitude and pre-strained under compression stress). The fractography shows that failure started in a pit and was propagated by fatigue. The dimensions of this pit were estimated by image analysis using SEM, having a depth of approximately 46 μm and a width of 104 μm.

Clear signs of localized corrosion caused by pitting, and cracks originating from pits, can be found on the surface of specimens near the primary fracture, as shown in Fig. 8 (c) and (d). Cracks and corrosion pits were seen in the pre-strained under tension stress specimen with 106,346 cycles (9.8 h under 425 MPa stress amplitude) and in the solution-treated specimen with 126,267 cycles (11.7 h under 325 MPa stress amplitude), respectively. Thus, it was clear that localized corrosion that only occurred under the effect of cyclic surface strain caused the reduction of fatigue strength.

4. Discussion

4.1. Material quality

ASS chemical composition within the parameters is very important to material corrosion resistance. The Cr and Mo contents are fundamental for localized corrosion resistance [32]. In addition, the chemical control ensures that the material will continue austenitic during hardening processing with a paramagnetic structure [2,33].

The inclusion content result (Fig. 4a) is compatible with the alloy fabrication by vacuum remelting process, which results in low inclusion content. The low amount of inclusions is a requisite for corrosion resistance of stainless steels since interfaces between matrix and

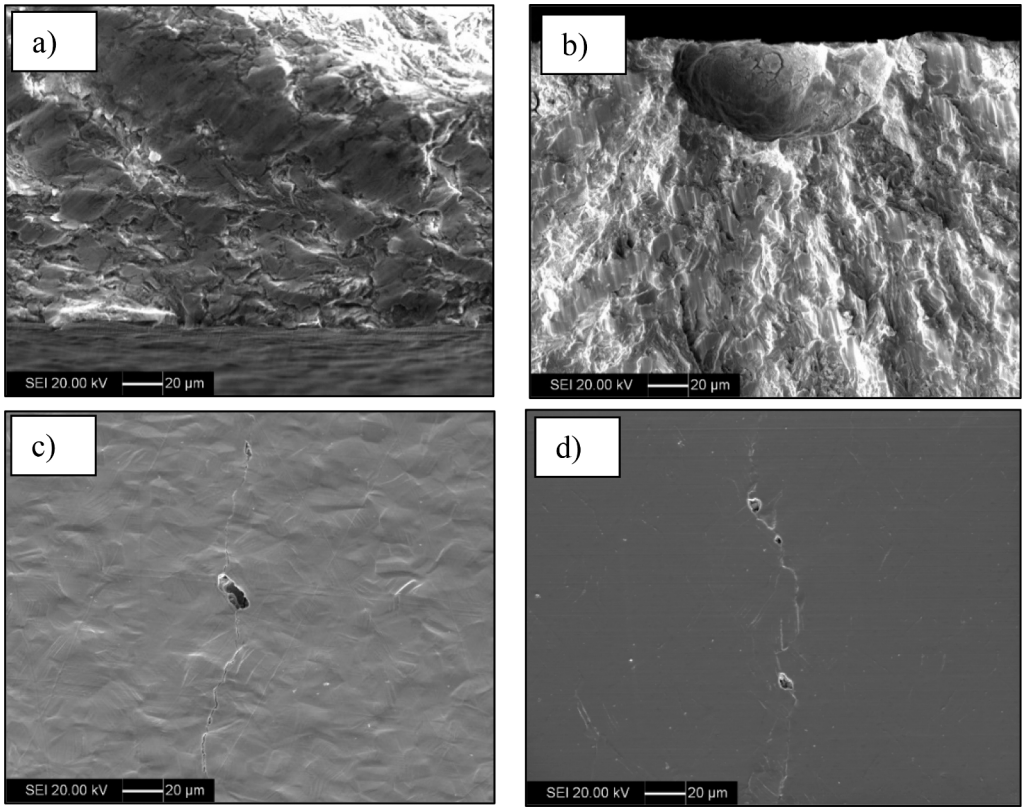

Fig. 8. Micrographs obtained by SEM showing: a) PPUT specimen failed after 199,912 cycles (18.5 h under 425 MPa stress amplitude, PBS solution). b) PPUC specimen failed after 81,088 cycles (7.5 h under 425 MPa stress amplitude, SHA solution). c) PPUT specimen failed after 106,346 cycles (9.8 h under 425 MPa stress amplitude, SHA solution). d) SPC specimen failed after 126,267 cycles (11.7 h under 325 MPa stress amplitude, SHA solution).

inclusions are preferential sites for nucleation of localized corrosion [30,34–36]. It is important to note the absence of sulphide inclusions, which are easily dissolved in the chloride test solution [37] and, therefore, can reduce the ASS corrosion resistance. Thus, the inclusions content in the studied ASS must not be a determinant factor in the corrosion-fatigue results since it is within the standard limits and will affect all conditions similarly. The microstructure (Fig. 4b) is expected for this material in the solution-treated condition, as received.

The localized hardening process through uniaxial stress was successful and consistent with applied cold work during pre-strain, either by compression or tension stresses, resulting in a similar hardening effect on both pre-strained specimens. Microstructure (Fig. 4c, d) is compatible with the 15% applied pre-strain, where a slight deformation of the austenitic grains is shown. Hardness values presented low scatter, showing that the pre-strain used, in tension or compression, resulted in similar homogenous strain hardening, indicating the effect of plastic pre-strain either by tension or compression on the corrosion fatigue of the ASS.

It is noted that this hardening produced a yield limit increase since the new yield limit after pre-strain can be assumed as the higher absolute true stress value reached in the pre-strain procedure (Fig. 5a), placing the material in a mechanical resistance condition compatible with the application requirements, above 690 MPa.

4.2. Pre-strain mechanical behavior effect

As shown in Fig. 5 b to d, high surface roughness was produced as a function of pre-strain. Together with data in Table 3, these observations illustrate how a polished surface is altered by deformation, leading to a new surface that may present a different interaction with the corrosive medium relative to the polished surface and possibly modify the fatigue nucleation mechanism. It must be noted that a large increase in roughness was caused by pre-strain, either by compression or tension stress. However, as seen in Table 3, the increase in roughness in compression was higher (250 nm) than in tension (110 nm).

Cold working increases the fatigue strength of stainless steel when the cyclic variation is predominantly elastic [38]. However, the increased roughness effect can be harmful to fatigue resistance. It is known that increased surface roughness reduces fatigue life compared to the same material but polished [39–41]. Thus, concerning the type of strain, compressive or in tension, it would be expected that compressive strain has a more harmful effect on fatigue resistance than tension strain due to the slightly higher roughness generated by surface extrusions in the compressive pre-strained samples. Following the pre-strain, there was a change in the residual stress located in the longitudinal direction. The stresses became more compressive with the compression and tractive with the tensile strain (Table 3). These changes in the residual stress profile influenced fatigue corrosion behaviour and will be addressed in the subsequent text.

4.3. Corrosion-fatigue behavior

The effect of hardening on corrosion-fatigue life in PBS solution was presented in Fig. 6a, which shows a significant increase in resistance concerning the solution-treated condition. Similar effects of increased corrosion-fatigue resistance by hardening were observed in SHA solution, Fig. 6b. Those results from cold working, which increases hardness and yield limit and, consequently, fatigue resistance, were expected due to hindering plastic strain mechanisms that generate fatigue failures.

PPUC specimens in PBS solution had low fatigue life compared to PPUT specimens in the same solution, corresponding to the expected due to its slightly higher surface roughness (Table 3). In the SHA solution, this roughness effect is not significant, probably, due to the overlapping of solution corrosiveness and the occurrence of pitting (Fig. 8b to d). Fatigue life is reduced in SHA solution comparatively to PBS solution in all conditions (Fig. 7a, b and c). The decrease in fatigue resistance exponent b in the SHA solution shows the corrosiveness effect of this test solution, showing the possible influence of pitting corrosion on fatigue resistance. A decrease in stress resulted in fewer cycles of failure in the SHA solution compared with the PBS solution.

In the three tested conditions (SPC, PPUT and PPUC), fatigue strength exponent, b, showed a decrease in SHA solution (see Table 4). Still, the largest decline was related to the pre-strained under tension stress (-0.040). The fatigue strength exponent decreased by approximately −0.028 and −0.014 for the solution-treated and pre-strained under compression stress specimens. This fact shows that pre-strained under compression stress specimens promoted a better corrosion-fatigue resistance in SHA solution.

Fatigue exponent drop (Table 4) shows a small range in PBS solution, −0.006. However, there is a slight tendency of medium aggressiveness on pre-strain under tension and compression specimens; b tends to be lower, respectively, −0.059 and −0,061. Those occurrences agree with the roughness increase and corrosive medium presence in the absence of localized corrosion (Fig. 8a). In the SHA solution, the variation was higher, −0,024, showing that the medium aggressiveness enhances the attack on tension pre-strain specimens, where b tends to be smaller (-0,099). However, pre-strained under compression stress specimens tend to be more resistant to corrosion fatigue, with a slightly higher b (-0,075), which suggests a delay in the pitting formation in these conditions.

According to the literature [42,43], reducing the interatomic surface spacing due to compressive stress helps the growth and maintenance of the passive film. Electrochemical impedance spectroscopy and X-ray photoelectron spectroscopy carried out in the same material used in this work with PBS solution showed a positive effect of the compressive loading on the corrosion resistance of the steel. The passive current density (i_{pass}) decreased for the strained samples, especially for that subject to 15% compressive deformation, for which i_{pass} was 63% lower for the solution-treated steel (as-received steel). The passive film formed at this condition presented strong Cr_2O_3 enrichment [43]. Thus, it is expected that compressive residual stress might increase the mechanical properties and the corrosion resistance of the ASS. This study corroborates the literature since compression pre-strain had a beneficial effect on the corrosion-fatigue resistance of the ASS. Besides, the density of defects (dislocation density) in the passive film is influenced by the defects at the alloy surface. In this way, pre-strain leads to increased defects in the passive film and, consequently, reduced corrosion resistance [44]. The results indicated that the corrosion-fatigue resistance depends on the type of plastic strain, and pre-strain under tension stress results in a passive film of lower resistance than that resulting from pre-strain under compression stress. One of the possible explanations for this behavior is that pre-strained under tension stress tends to affect the interface between inclusions and matrix, increasing the susceptibility of these sites to the nucleation of corrosion pits [45]. However, this material has a low level of inclusions to ensure that this mechanism is less important in this ASS.

The study results evidenced that plastic strain affects the passive film structure and, consequently, its corrosion resistance since tension plastic pre-strain increased the susceptibility to corrosion of the ASS during corrosion-fatigue tests in a more aggressive environment.

When comparing the fatigue life reduction due to the corrosiveness

Table 4
Fatigue strength exponent (b) for the various specimens and solutions used in the corrosion-fatigue tests.

Specimen	b_1 – PBS solution	b_2 – SHA solution	b_2-b_1
SPC	−0.055	−0.083	−0.028
PPUC	−0.061	−0.075	−0.014
PPUT	−0.059	−0.099	−0.040
Same solution range	−0,006	−0,024	–

of solutions (SHA solution compared to PBS solution), Fig. 7a-c, using 300,000 cycles corrosion-fatigue life, it is observed that solution-treated samples underwent higher stress fatigue life reduction (11%) compared to the pre-strained under tension stress samples (8.6%) and pre-strained under compression stress ones (2%). However, considering higher fatigue lives, the fatigue resistance exponent b decay causes a higher reduction for pre-strained under tension stress samples.

Cold working has been related to the increased corrosion resistance of steel. This increased corrosion resistance was associated with more pitting nucleation sites and pitting depth reduction on cold-worked materials [4,46]. However, this finding does not consider the effect of surface roughness since, in both articles [4,46], the samples are usually polished after cold work and before corrosion tests.

Plastic strain also affects the passive film properties, improving the film's resistance to corrosion attack. Passive film protection improved by cold working was attributed to increased density of low-angle grain boundaries and dislocations. A high density of defects can promote the diffusion of Cr to the surface, resulting in a Cr-enriched passive film of improved resistance to corrosion [47,48]. On the other hand, cold working can promote atomic disorder that weakens the atomic bond with the matrix [49,50]. Regardless of the mechanism, cold working improved the corrosion-fatigue properties of the ASS studied here.

The harmful effect of SHA caused by its high aggressiveness due to its low pH (pH 3), presence of H_2O_2 (1%) and albumin (1%), typical of inflammatory reactions in the implanted region and crevice conditions, showed that fatigue strength limit reduction occurs under such conditions and reduced localized corrosion resistance. However, these work observations did not indicate how PBS accelerated fatigue failure. Nevertheless, the PBS interaction with specimens decreased their fatigue life even though, under such test conditions, surface pitting was not found.

The literature [48] reported high cycle fatigue tests in Ringer's solution and air and showed a 21% decrease in fatigue life in the solution compared to air. There were no surface defects due to localized corrosion, like visible pits in the fracture image, but fatigue life reduction was observed.

Corrosion-fatigue crack initiation is not only enhanced by pitting corrosion. Cyclic loading that breaks a passive oxide film formed at every loading cycle can also affect fatigue life. This effect produces roughness in a localized way and locates the defects that will start the crack [16–18].

The failure due to fatigue comes from persistent slip bands (PSBs) that produce extrusions and intrusions, where, from an intrusion, a crack can nucleate. At these points, there is localized plastic strain. It is important to point out that this mechanism will always happen. When there is a corrosion pit, a bottom pit stress concentration will cause localized plastic strain. Even in the absence of pits, when surface roughness occurs from successive breaks of the passive film by cyclic load [16–18], in the same way, the points most harmed by this phenomenon will cause stress concentration and localized plastic strain.

If the fatigue test was performed under vacuum, slipping between planes during the loading cycle produces steps on the surface. During the unloading cycle or subsequent compression, these steps are reverted by reverse slip, creating a random surface roughness. These continued processes will produce an intrusion in the PSBs that will start the cracks. In aggressive environments or air, the chemisorption of species (or formation of oxide film) in the newly formed slips reversed steps is most difficult in the same slip plane. Thus, aggressive environments promote a surface roughness increase mechanism and species transport into the surface close to the PSBs that will facilitate crack initiation [18,19,51–53], explaining the decrease in fatigue life under corrosive solutions even in the absence of localized corrosion. The increased roughness of the pre-strained specimens under compression stress corroborates this mechanism in PBS solution since fatigue resistance reduction also occurred in this solution (Fig. 8a).

The literature reported that hemispherical defects with a 95 μm diameter reduce fatigue stress limit by approximately 9% [54,55]. Thus, as found in this study, pits might be responsible for the fatigue life decrease in the SHA solution. Fig. 8b to d showed that there was a change in corrosion form due to SHA solution: a more consistent corrosion form that reduces fatigue life, pitting corrosion, which is more detrimental to implant devices since it locally removes mass, producing a stress concentration point that abbreviates initial crack nucleation.

Since the SHA solution did not produce corrosion pits in the previous three weeks of conditioning, it is believed that the main factor for the pit's appearance was the cyclic loading. The cyclic stress below the yield limit has no obvious influence on the rate of metastable pits since it presents little difference from the static behavior. However, upper yield limit, a remarkable increase in metastable pits events is observed, approximately 1.8 times higher than in the absence of cyclic loading [15]. Thus, points at PSBs and PSMBs have plastic strain (stress upper yield limit), undergoing an increase of metastable pits events. Although this solution does not cause the pit formation without cyclic loading, in its presence and at a certain fatigue life instant, conditions of stress concentration that gave rise to pits formation lead them to their critical size, developing the cracks.

However, why was there no pit corrosion in the PBS solution? This answer can only be attributed to the SHA solution's strong corrosivity contribution. The pH decrease places the material in an imminent activation condition to release corrosion products instead of a passive film formation [10,56]. H_2O_2 and albumin combination leads to a total concentration of released metals, which is even higher than the sum of both effects, H_2O_2 and albumin, isolated, which means that H_2O_2 and albumin exert a synergistic harmful impact on the corrosion of stainless steel [7]. Those conditions are present in the SHA solution. Together with the cyclic load, the failure process changed to corrosion pits and subsequent fatigue cracks appearance from these pits, reducing the fatigue life of ASS implant material in the SHA solution.

5. Conclusions

The studied ASS ISO 5832-1 presented a homogeneous microstructure composed of austenite grains and intragranular twins with low content of inclusions compatible with its manufacturing process by vacuum remelting.

Pre-strain induced a homogeneous and similar strain hardening in the corrosion-fatigue test specimens. This pre-strain also increased surface roughness. Compression pre-strain produced surface roughness are slightly higher than tension pre-strain.

The material fatigue resistance was increased by pre-strain. In a PBS solution, the increase was higher for the specimens pre-strained under tension stress.

In the SHA solution, fatigue life was reduced in all tested conditions. Besides, pre-strain under compression or tension stresses had similar effects on fatigue life. However, pre-strain under tension strain showed a higher tendency for fatigue resistance decrease with an increasing number of cycles, indicated by the fatigue exponent strength decay.

Corrosion pits were induced in the SHA solution and accelerated corrosion-fatigue failure in all tested specimens. Pitting-inducing factors were cyclic load, low pH and the synergic effect of H_2O_2 and albumin.

Data availability

Data will be made available on request.

Declaration of Competing Interest

The authors declare that they have no known competing financial interests or personal relationships that could have appeared to influence the work reported in this paper.

Data availability

Data will be made available on request.

Acknowledgements

The authors thank Villares Metals for providing the steel used in this research. They are also grateful to IPEN and FEI for the availability of research facilities.

FAPESP Assistance: Process 2012/50187-7.

References

[1] Rodríguez-González, FA; ASM, I. Biomaterials in Orthopaedic Surgery. Materials Park, Ohio: ASM International, 2009. ISBN: 9781615030095.
[2] Woods TO. MRI Safety and Compatibility of Implants and Medical Devices, Stainless Steels for Medical and Surgical Applications. ASTM STP 1438, G. L. Winters and M. J. Nutt, Eds., ASTM International, West Conshohocken, PA, 2003.
[3] Pohler OE.Failures of Metallic Orthopedic Implants. In: Metals Handbook 11 – Failure Analysis and Prevention (pp. 2740-2790). NY: ASM International; (2002).
[4] Talha M, Behera CK, Kumar S, Pal O, Singh G, Sinha OP. Long term and electrochemical corrosion investigation of cold worked AISI 316L and 316LVM stainless steels in simulated body fluid. RSC Adv 2014;4(26):13340–9.
[5] Heurtault S, Robin R, Rouillard F, Vivier V. On the propagation of open and covered pit in 316l stainless steel. Electrochim Acta 2016;203:316–25.
[6] Yu F, Addison O, Davenport AJ. A synergistic effect of albumin and H2O2 accelerates corrosion of Ti6Al4V. Acta Biomater 2015;26:355–65.
[7] Xu W, Yu F, Yang L, Zhang B, Hou B, Li Y. Accelerated corrosion of 316L stainless steel in simulated body fluids in the presence of H2O2 and albumin. Mater Sci Eng C 2018;92:11–9.
[8] Brooks EK, Brooks RP, Ehrensberger MT. Effects of simulated inflammation on the corrosion of 316L stainless steel. Mater Sci Eng C 2017;71:200–5.
[9] Rozali AA, Masdek NRN, Murad MC, Salleh Z, Hyie KM. The effect of pH value on the corrosion behaviour of Ti-6Al-4V and 316L SS alloys under physiological environment. Chem Eng Trans 2018;63:769–74.
[10] Hallam P, Haddad F, Cobb J. Pain in the well-fixed, aseptic titanium hip replacement: The role of corrosion. J Bone Joint Surg British 2004;86(1):27–30.
[11] Konttinen YT, Takagi M, Mandelin J, Lassus J, Salo J, Ainola M, et al. Acid attack and cathepsin K in bone resorption around total hip replacement prosthesis. J Bone Miner Res 2001;16(10):1780–6.
[12] Takagi K, Yamaga M. A new, modified operation for funnel chest using the Zimmer osteosynthetic plate. Arch Orthop Trauma Surg 1986;105(3):154–7.
[13] Talha M, Ma Y, Lin Y, Mandal AK, Sinha OP, Kong X. Corrosion performance of various deformed surfaces of implant steel for coronary stent applications: Effect of protein concentration. Colloids Surf B Biointerfaces 2021;197:111407.
[14] Polak J, Man J. Experimental evidence and physical models of fatigue crack initiation. Int J Fatigue 2016;91:294–303.
[15] Guan L, Zhang B, Yong XP, Wang JQ, Han EH, Ke W. Effects of cyclic stress on the metastable pitting characteristic for 304 stainless steel under potentiostatic polarization. Corros Sci 2015;93:80–9.
[16] Maruyama N, Mori D, Hiromoto S, Kanazawa K, Nakamura M. Fatigue strength of 316L-type stainless steel in simulated body fluids. Corros Sci 2011;53(6):2222–7.
[17] Nový F, Zatkalíková V, Boků̊vka O, Miková K. Gigacycle fatigue endurance of marine grade stainless steels with corrosion pits. Period Polytech Transp Eng 2013;41(2):99–103.
[18] Cahn RW, Haasen P. Physical metallurgy. 4. ed. Amsterdan: Elsevier Science B. V., v. 3, 1996.
[19] Suresh S. Fatigue of materials: 2. ed. Cambridge: Cambridge University, c1998.
[20] Boesmueller S, Baumbach SF, Hofbauer M, Wozasek GE. Plate failure following plate osteosynthesis in periprosthetic femoral fractures. Wien Klin Wochenschr 2015;127(19):770–8.
[21] ASTM E1097-12 Standard Guide for Determination of Various Elements by Direct Current Plasma Atomic Emission Spectrometry, ASTM International, West Conshohocken, PA, 2012, 10.1520/E1097-12.
[22] ASTM E1019-11 Standard Test Methods for Determination of Carbon, Sulfur, Nitrogen, and Oxygen in Steel, Iron, Nickel, and Cobalt Alloys by Various Combustion and Fusion Techniques, ASTM International, West Conshohocken, PA, 2011, 10.1520/E1019-11.
[23] ASTM E3-11(2017), Standard Guide for Preparation of Metallographic Specimens, ASTM International, West Conshohocken, PA, 2017, www.astm.org.
[24] ASTM E45-18a, Standard Test Methods for Determining the Inclusion Content of Steel, ASTM International, West Conshohocken, PA, 2018, www.astm.org.
[25] ASTM E112-13(2021) Standard Test Methods for Determining Average Grain Size, ASTM International, West Conshohocken, PA, 2013, DOI: 10.1520/E0112-13R21.
[26] ASTM E8/E8M-16a Standard Test Methods for Tension Testing of Metallic Materials, ASTM International, West Conshohocken, PA, 6, 10.1520/E0008_E0008M-16A.
[27] ASTM E466-15 Standard Practice for Conducting Force Controlled Constant Amplitude Axial Fatigue Tests of Metallic Materials, ASTM International, West Conshohocken, PA, 2015, 10.1520/E0466-15.
[28] ASTM E9-09(2018) Standard Test Methods of Compression Testing of Metallic Materials at Room Temperature, ASTM International, West Conshohocken, PA, 2018, 10.1520/E0009-09R18.
[29] ASTM E384-17 Standard Test Method for Microindentation Hardness of Materials, ASTM International, West Conshohocken, PA, 2017, 10.1520/E0384-17.
[30] ISO 5832-1 Implants for surgery – Metallic materials – Wrought stainless steel, International Standard, Switzerland, 2007.
[31] ASTM E739-10(2015), Standard Practice for Statistical Analysis of Linear or Linearized Stress-Life (S-N) and Strain-Life (ε-N) Fatigue Data, ASTM International, West Conshohocken, PA 19428-2959. United States.
[32] ASM Specialty Handbook. Stainless Steels. ASM International, 1994.
[33] KRAUSS, George. **Steels**: processing and performance. Ohio: ASM International, 2005.
[34] Man C, Dong C, Liu T, Kong D, Wang D, Li X. The enhancement of microstructure on the passive and pitting behaviors of selective laser melting 316L SS in simulated body fluid. Appl Surf Sci 2019;467:193–205.
[35] Jaimes RFVV, de Andrade Afonso MLC, Rogero SO, Agostinho SML, Barbosa CA. New material for orthopedic implants: Electrochemical study of nickel free P558 stainless steel in minimum essential medium. Mater Lett 2010;64(13):1476–9.
[36] Yang H, Yang K, Zhang B. Pitting corrosion resistance of La added 316L stainless steel in simulated body fluids. Mater Lett 2007;61(4–5):1154–7.
[37] Wang Y, Akid R. Role of nonmetallic inclusions in fatigue, pitting, and corrosion fatigue. Corrosion 1996;52(02).
[38] Misra RDK, Nune C, Pesacreta TC, Somani MC, Karjalainen LP. Understanding the impact of grain structure in austenitic stainless steel from a nanograined regime to a coarse-grained regime on osteoblast functions using a novel metal deformation–annealing sequence. Acta Biomater 2013;9(4):6245–58.
[39] Xie X, Ning D, Sun J. Strain-controlled fatigue behavior of cold-drawn type 316 austenitic stainless steel at room temperature. Mater Charact 2016;120:195–202.
[40] Lai J, Huang H, Buising W. Effects of microstructure and surface roughness on the fatigue strength of high-strength steels. Procedia Struct Integrity 2016;2:1213–20.
[41] Barriuso S, Chao J, Jiménez JA, García S, González-Carrasco JL. Fatigue behavior of Ti6Al4V and 316 LVM blasted with ceramic particles of interest for medical devices. J Mech Behav Biomed Mater 2014;30:30–40.
[42] Takakuwa O, Soyama H. Effect of Residual Stress on the Corrosion Behavior of Austenitic Stainless Steel. Adv Chem Eng Sci 2015;5:62–71. https://doi.org/10.4236/aces.2015.51007.
[43] dos Santos RCF, Naville W, de Lima NB, Costa I, Antunes RA. On the Interaction between Uniaxial Stress Loading and the Corrosion Behavior of the ISO 5832–1 Surgical Stainless Steel. J Mater Eng Perform 2021;30(4):2691–707.
[44] Tandon V, Patil AP, Rathod RC. Correlation of martensite content and dislocation density of cold worked 316L on defect densities of passivating film in acidic environment. Mater Res Express 2018;5(8):086515.
[45] Ramirez AH, Ramirez CH, Costa I. Cold rolling effects on the microstructure and pitting resistance of the NBR ISO 5832–1 austenitic stainless steel. Int J Electrochem Sci 2014.
[46] Muley SV, Vidvans AN, Chaudhari GP, Udainiya S. An assessment of ultra fine grained 316L stainless steel for implant applications. Acta Biomater 2016;30:408–19.
[47] Tanhaei S, Gheisari K, Alavi Zaree SR. Effect of cold rolling on the microstructural, magnetic, mechanical, and corrosion properties of AISI 316L austenitic stainless steel. Int J Miner Metall Mater 2018;25(6):630–40.
[48] Ahmed AA, Mhaede M, Wollmann M, Wagner L. Effect of surface and bulk plastic deformations on the corrosion resistance and corrosion fatigue performance of AISI 316L. Surf Coat Technol 2014;259:448–55.
[49] Fu Y, Wu X, Han EH, Ke W, Yang K, Jiang Z. Effects of cold work and sensitization treatment on the corrosion resistance of high nitrogen stainless steel in chloride solutions. Electrochim Acta 2009;54(5):1618–29.
[50] Chen J, Xiao Q, Lu Z, Ru X, Han G, Tian Y, et al. The effects of prior-deformation on anodic dissolution kinetics and pitting behavior of 316L stainless steel. Int J Electrochem Sci 2016;11(2):1395–415.
[51] Kubin LP, Estrin Y. Strain nonuniformities and plastic instabilities. Revue de physique appliquée 1988;23(4):573–83.
[52] Kubin LP, Devincre B. From dislocation mechanisms to dislocation microstructures and strain hardening. Deformation-Induced Microstructures: Analysis and Relation to Properties. 1999:61–83.
[53] Bolton JD, Redington ML. The effects of saline aqueous corrosion on fatigue crack growth rates in 316 grade stainless steels. Int J Fatigue 1983;5(3):155–63.
[54] Guerchais R, Morel F, Saintier N, Robert C. Influence of the microstructure and voids on the high-cycle fatigue strength of 316L stainless steel under multiaxial loading. Fatigue Fract Eng Mater Struct 2015;38(9):1087–104.
[55] Guerchais R, Morel F, Saintier N. Effect of defect size and shape on the high-cycle fatigue behavior. Int J Fatigue 2017;100:530–9.
[56] Caballero Sarmiento J, Correa Munoz E, Estupinan Duran H. Analysis of the biocompatibility of Ti6Al4V and stainless steel 316 LVM based on effects of pH, applying criteria of ASTM F2129 standard. Ingeniare Revista Chilena de Ingeniería 2017;25(1):95–105.